Efficiency Justification for Modernizing a Grain Screw Extruder to Produce Feed Additives from Crop Residues

Mikhail Doudkin
International School of Engineering, D. Serikbayev East Kazakhstan Technical University, Kazakhstan
mdudkin@ektu.kz

Alina Kim
Miras University, Kazakhstan
alinakim3107@gmail.com (corresponding author)

Andrey Vavilov
LLP Scientific and Production Association INNOTECH, Kazakhstan
avavilov@ektu.kz

Georgy Guryanov
LLP Scientific and Production Association INNOTECH, Kazakhstan
gguryanov@ektu.kz

Vladimir Yakovlev
International School of Engineering, D. Serikbayev East Kazakhstan Technical University, Kazakhstan
vjakovlev@ektu.kz

Yevgeniy Varavin
Business School, D. Serikbayev East Kazakhstan Technical University, Kazakhstan
evaravin@edu.ektu.kz

Received: 1 July 2025 | Revised: 20 July 2025 | Accepted: 2 August 2025

Licensed under a CC-BY 4.0 license | Copyright (c) by the authors | *DOI: https://doi.org/10.48084/etasr.13086*

ABSTRACT

This study presents a scientific and experimental justification for improving the design of a grain screw extruder for processing crop and forestry residues. The screw assembly is the core and most sensitive part of any extruder. To transform the initial feed mixture into the finished product at the extruder output, the material passes through a series of technological processes along the screw length. The accomplishment of these processes over a shorter screw length—without compromising the product quality—reduces the processing time, construction costs, and energy consumption, while it increases productivity. This research evaluates the potential for performance improvement through modifications to the screw assembly. The justification for modernization began with theoretical investigations. Both existing and newly derived analytical equations were used to assess the screw design and its impact on the performance and efficiency when processing crop residues and ground Siberian fir needles. The study also validates the structural integrity, functionality, and technological feasibility of the modernized extruder system. The upgraded extruder was tested on a feed mixture of crushed sunflower stalks and heads, as well as fir needles, which are rich in minerals and vitamins. The tests showed that the extruder's operation is virtually independent of the feedstock composition. The machine can be adjusted to process any type of crushed plant residue, significantly simplifying the raw material preparation for extrusion.

Keywords-extruder; extruder screw; double-entry screw; compression rings; inter-turn spacing; screw pitch; die plate

I. INTRODUCTION

Every feed producer strives to provide a stable supply of high-quality, cost-effective, and palatable animal feeds in various forms for agricultural livestock. To achieve this, priority is often given to reducing the production costs by lowering the price of the raw materials. Crop residues—such as sunflower stalks, heads, and press cake — and forestry by-products, like shredded Siberian fir needles, are usually treated as waste and can be obtained at minimal cost. These materials can be added to conventional feed formulations in amounts up to 20%, enriching them with natural minerals and vitamins while lowering the overall cost of the feed components.

Grains remain the primary filler in most compound feeds, making the physical methods of grain preparation and processing the most widely used. Today, more than ten such methods are utilized, which require various machines, including crushers, mills, flakers, mixers, shredders, and others [1-4].

Using different types of equipment, grain can be boiled, steamed, treated with hot air, roasted, flaked, pelletized, micronized, or extruded. While many operational and maintenance issues related to these machines have been addressed, some remain unresolved and require scientific justification to guide the modernization efforts aimed at enhancing the productivity and efficiency of the existing technologies.

The present article presents the results of research on the modernization of the compact grain extruder PE-150, as shown in Figure 1, produced by the Kostanay-based company LLP "AGROTECHSERVICE 12" in Kazakhstan. The design principles discussed can also be applied to other types of extruders. The use of an extruder makes it possible to combine a sequence of operations–mixing multiple components, grinding, compressing, flattening, heating, cooking, steaming, sterilizing, coloring, and forming–into a single continuous process.

The grain extrusion technology is typically classified into two groups: dry extrusion and wet extrusion. The difference lies in the moisture content of the raw material before it enters the extruder. Dry extrusion is used when the material has a moisture content of up to 15%, while wet extrusion is used for materials with moisture levels above 15%. Dry extrusion is a simpler method, where the feed mixture enters the extruder directly and is processed under temperatures up to 150°C and pressure of up to 4 MPa. This method is widely used in feed production due to its relatively low energy consumption (80–120 kWh/ton). However, a drawback of dry extrusion is the shortened service life of the screw assembly components. The initial operational lifespan of the PE-150 extruder is 350–600 h, while other models range between 600–1200 h–significantly lower than the lifespan of wet-type extruders, which can reach 8000–10000 h. Another notable disadvantage of dry extruders is their lower productivity and instability of the working process.

Properly selected extruder parameters can reduce the processing time, improve the process conditions, enhance the feed quality, and extend the shelf life of the feed and feed additives.

The extrusion process and the operational principles of various extruders have been thoroughly studied [5-12].

Fig. 1. Grain Extruder PE-150 (assembled).

Authors in [13] studied the reliability of the screw and frame of an extruder used in the production of biodiesel from castor seeds (Ricinus communis). They focused on the deformation behavior of the screw and frame under different loads and explored the extruder's ability to efficiently process various seeds, grains, and plant materials. Their work resulted in safe operating parameters and screw design recommendations. Authors in [14] improved screw designs for processing biogas slurry into organic fertilizers, testing over ten different screw configurations and identifying the most effective one for specific feedstock parameters.

Authors in [15] analyzed the failures in twin-screw extruder shafts and concluded that the fatigue failure caused by torsional and bending loads, which had not been properly accounted for during manufacturing, led to breakdowns. Following the shaft restoration, they proposed recommendations for the screw shaft design and operation. Authors in [16] used 3D finite element modeling to identify the critical stress-deformation states in extruder shaft fastening areas and calculated the maximum stress intensities along keyway edges. Their work contributed valuable insights for optimizing the shaft geometry and operating conditions.

Authors in [17] justified the extruder parameters and proposed improvements in the design and extrusion process for sapropel-grain feed mixtures. They focused on screw sections with varying pitch distances to improve the extruder productivity. Authors in [18] conducted finite element analysis of a worm screw used in meat grinders and found that increasing the inter-pitch volume could enhance the plastic deformation rates. Based on these results, they proposed structural modifications. Authors in [19], using ANSYS static structural analysis, explored the causes of low efficiency and screw shaft failures. Despite the high cost of materials, they

concluded that replacing the screw shaft material was a more cost-effective strategy, reducing the maintenance and productivity losses. Several upgraded screw shaft designs were proposed and evaluated.

These studies build upon the foundational work of early mechanical engineers who pioneered the development of feed production machinery. However, earlier research largely focused on homogeneous feedstocks with consistent properties. The current study, in contrast, proposes a modernization of the extruder design, capable of reliably processing a wider variety of feed mixtures, including those enriched with low-cost crop and forestry residues. If poorly processed, such additives can negatively affect the strength, hardness, consistency, appearance, and palatability of compound feeds [20-22].

The efficiency of the proposed extruder modernization was verified using the Python and MATLAB software. The study addresses the specific challenges of processing the plant waste at the local level, where such materials are abundant. This approach, through the partial substitution of traditional grain fillers, helps address both the economic and ecological challenges.

Feeding cattle with extruded feed can increase the milk yields by 25–30% and live weight gains by 10–20%. However, despite these benefits, the production of extruded feed remains a budget-intensive process. Therefore, reducing the feed production costs is a critical part of the equipment and process design [23].

The aim of this study is to modernize and scientifically justify the design and technological parameters of the screw assembly in a grain extruder, as well as to improve the extrusion process for feed mixtures with added crop residues [24, 25]. Achieving this goal will help eliminate the need for costly trial-and-error approaches when upgrading other extruder systems, thereby increasing the predictability and efficiency in feed machinery development.

II. METHODOLOGY AND RESEARCH PROCEDURE

The screws, shaft, and screw casing are the key extruder components that affect the production process the most and need the most frequent maintenance or repair. These parts also require particularly close monitoring and maintenance. It is essential to ensure that the raw material being processed meets the quality and moisture specifications. An undersized or overdried input material can lead to failure or breakage of the shaft or screws. In contrast, an overly moist material can cause steam micro-explosions at the extruder outlet, the recoil of which may also damage the shaft, screws, or body of the machine.

Single-screw extruders have gained wide adoption in the feed production industry due to their structural simplicity, relatively low energy consumption, and the significant reduction in the cost of the final feed product they offer.

The composition and main structural elements of the screw assembly of the grain extruder are shown in Figure 2.

The prepared mixture is fed from the hopper's dosing unit into the working zone between the extruder housing (3) and the screw (2), where it undergoes gradual compression and heating. Compression intensifies intermittently at the locations of the compression gate rings (6), which are sequentially mounted on the shaft (1) after each screw section (2). A portion of the processed mixture is forced through the gap between the housing (3) and the compression ring (6), while another portion is pushed backward and redirected via the horizontal return grooves (5) in the housing (3) back to the feed zone. There, it mixes with a new portion of the incoming mixture, re-enters the compression and heating zone, and is reheated due to the compression and frictional forces, then advanced forward by the screw flights (2), as shown in Figure 3.

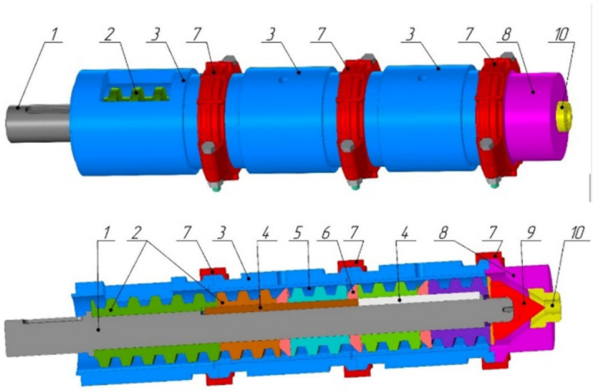

Fig. 2. Screw assembly (compression unit) of the extruder: 1 – screw shaft, 2 – feeding screw, 3 – housing, 4 – key, 5 – horizontal grooves of the housing, 6 – compression gate, 7 – coupling, 8 – die head, 9 – conical tip, 10 – die plate (nozzle).

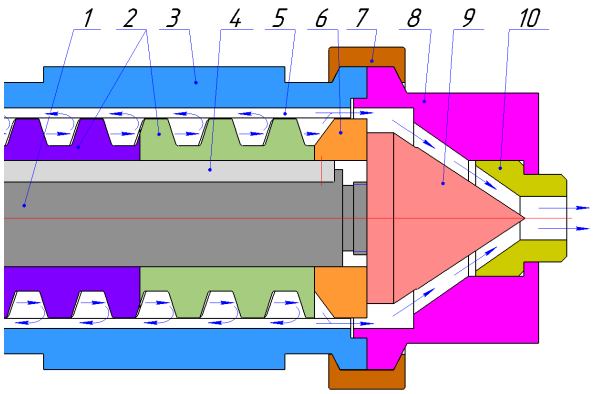

Fig. 3. Feed movement process in the pe-150 press extruder: 1 – screw shaft, 2 – feeding screw, 3 – housing, 4 – key, 5 – horizontal grooves in the housing, 6 – compression gate, 7 – coupling, 8 – die head, 9 – conical tip of the shaft, 10 – die plate.

As the mixture passes through the gap between each compression ring (6) and the housing (3), the material undergoes structural transformation under shear stress and friction, with a simultaneous rise in temperature, leading to the melting of the mixture. The finished feed product exits the screw zone of the extruder through the die orifice (10) in the die head (8). The diameter and cross-sectional area of the die opening (10) can be adjusted via controlled tightening.

Changing the cross-sectional area of the die affects the overall pressure and temperature of the feed mixture in the screw zone of the extruder. The working pressure must be sufficient to extrude the molten feed product through the die opening (10), where it expands in volume due to "explosive" steam microbursts at the outlet.

As a result of analytical and experimental investigations, a hypothesis was formulated: the width of the compression rings (6) and their angle of inclination toward the inner surface of the housing (3) have a significant influence on the pressure and temperature parameters of the feed mixture passing through them. In all feed extruders, the primary working component is a solid or modular screw, whose parameters significantly affect both the energy consumption and the quality of the final feed product. The screw operates along the entire length of the feedstock's path through the extruder. Initially, it captures the raw material from the hopper's feeder, mixes it, transports it forward, compresses, presses, propels, and contributes to the heating, thermal treatment, and melting of the mixture, finally pushing it through the die opening.

The screw shaft is assembled in sections, with each section representing a segment of the modular screw separated by compression rings. Each section of the screw corresponds to a specific functional zone. In the first zone (the intake zone), the raw feed mixture is captured, further mixed, initially compressed, and transferred to the next zone–the feeding zone –where the components begin to mechanically break down, compact intensively, get pressed, heated, melted, and undergo shear-induced plastic deformation.

The third zone, known as the compression or pressing zone, is responsible for homogenizing the mixture and extruding it under high pressure through the die opening. Since the tasks of the screw vary in each zone, the screw shaft is made modular, with tailored characteristics for each section. This modular design allows the parameters of each screw section to be optimized individually, thereby ensuring the most efficient operation of each functional zone. To achieve this, the present study established three research objectives:

- To investigate the influence of the screw pitch on the productivity and efficiency, and determine the optimal screw pitch in each processing zone.
- In zones 2 and 3, to evaluate the impact of a single-shaft double-entry screw on the extrusion efficiency.
- To analyze the effect of the design parameters and shape of the compression gate rings on the extruder's performance and structure.

To determine the optimal operational parameters of the extruder (pressure, temperature, throughput), the working process of the modernized extruder design was mathematically modeled. The structural and technological parameters influencing the efficiency of the extruded feed production with the inclusion of crop residues were also defined. To calculate the required extrusion pressure P_p for the feed mixture discharge (or "ejection"), the study considered the movement of the mixture through the annular conical channel of the die, as shown in Figure 4. The forces acting on an elementary layer of the compressed fibrous-plant feed mixture with thickness dx at a distance x from the beginning of the channel are identified and balanced. The passage gap for the processed fibrous-plant mixture is formed between the conical surfaces of the die plate (10) and the conical tip of the shaft (9), as can be seen in Figure 3.

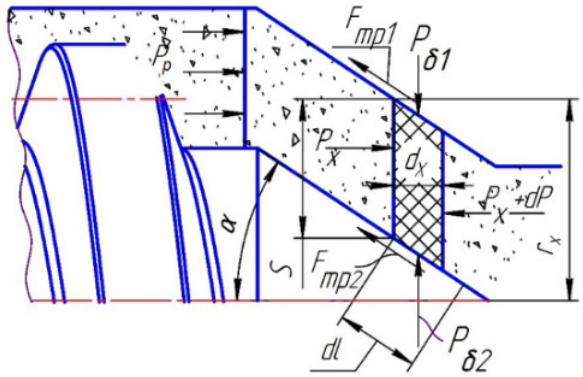

Fig. 4. Material flow in the forming die head.

For an elementary layer of thickness dx a differential equilibrium equation is constructed with respect to the horizontal X-axis:

$$P_x(2\pi S r_x - nS^2) - (P_x + dP)\pi(2\pi S r_x - nS^2) - F_{tr1}cos\alpha - F_{tr2}cos\alpha = 0 \quad (1)$$

where P_x is the pressure at the current section of the channel in (Pa), F_{tr1} and F_{tr2} are the friction forces on the die wall and shaft surface, respectively (N), S is the clearance between the die and the shaft (m), and r_x is the radius of the current channel section (m).

The friction force is expressed in terms of lateral pressure:

$$F_{tr1} = 2\pi \cdot r_x \cdot dl \cdot f \cdot P_{b1}cos\alpha \quad (2)$$

$$F_{tr2} = 2\pi \cdot (r_x - S) \cdot dl \cdot f \cdot P_{b2}cos\alpha \quad (3)$$

where P_{b1} and P_{b2} are the lateral pressure on the current section of the channel along the die wall and shaft surface, respectively, (Pa), d_l is the width of the selected conical section (m), α is the inclination angle of the generatrix of the cone (degrees), and f is the coefficient of friction (dimensionless).

In Figure 4, the width of the conical section is expressed through the thickness of the elementary layer dx and the inclination angle α of the generatrix of the cone:

$$dl = \frac{dx}{cos\alpha} \quad (4)$$

After applying the necessary transformations and taking into account (2), (3), and (4), the following expression is obtained:

$$dP\pi(2Sr_x - S^2) = 2\pi dx f P_{b1}cos\alpha(2r_x - S) \quad (5)$$

Assuming a linear relationship between the lateral pressure and the axial coordinate over the entire interval, the resulting equation is:

$$P_{b=}\xi \cdot P_x \quad (6)$$

where ξ is the lateral pressure coefficient, $\xi = \mu/(1+\mu)$, here representing the Poisson's ratio and P_x is the pressure in the die (at section dx), (Pa):

$$P_x = \frac{P_0}{e^{\frac{2\xi \cdot f \cos\alpha}{S}}} \quad (7)$$

where P_0 is the outlet pressure from the die (Pa), and X is the distance from the beginning of the channel to the pressure evaluation point (m).

Equation (7) can be used to determine the pressure at any point within the outlet section of the die. Using (7), the extrusion (ejection) pressure can be calculated as:

$$P_p = \frac{P_0}{e^{\frac{2\xi \cdot f \cos\alpha}{S}}} \quad (8)$$

where l is the axial length (extent) of the outlet channel (m).

For calculation convenience, the clearance S between the conical tip of the shaft and the die is expressed in terms of the cross-sectional area of the die outlet:

$$S_{otv} = \pi(2r_0 S - S^2) \quad (9)$$

where r_0 is the inner radius of the cylindrical screw housing (m).

Equation (8) demonstrates that the pressure required for extrusion depends on the geometric dimensions of the die, such as its length l and the inclination angle α of the cone generatrix. For the values α =300, ξ = 0.43, f = 0,4 and S_{otv} = 1,1 cm^2, theoretical data points were calculated to show the relationship between the extrusion pressure and the axial length l of the die. The trend shown in Figure 5 indicates that an increase in l leads to a corresponding increase in the extrusion pressure.

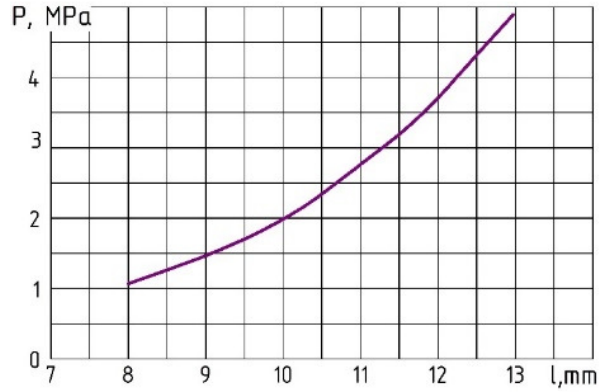

Fig. 5. Relationship between extrusion pressure P_p within the screw assembly and die length l.

This relationship enables the selection of a die length l during the design phase that ensures that the required extrusion pressure is achieved. Based on (9), Figure 6 illustrates the relationship between the cross-sectional area S_{otv} of the die outlet and the extrusion pressure P_p for the following parameters: α = 300, ξ = 0.43, f = 0.4, and l = 9 mm.

The trend in Figure 6 indicates that increasing the die outlet area results in a decrease in the extrusion pressure. This relationship can be used to regulate and maintain the overall pressure within the screw zone at a level sufficient for the proper extrusion of the final feed product.

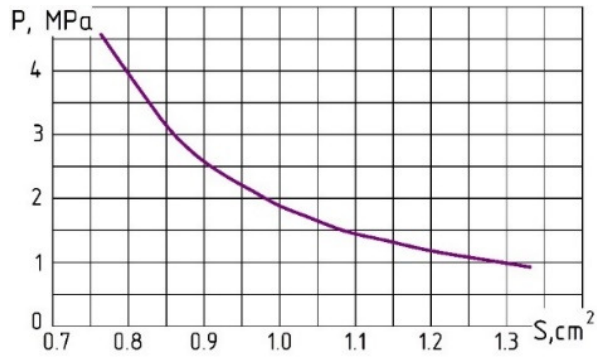

Fig. 6. Relationship between extrusion pressure Pp in the screw assembly and the cross-sectional area S_{otv} of the die.

To accelerate the increase in the internal screw pressure– and consequently the temperature of the feed mixture– compression gate rings are installed between the screw sections. The outer surface of these rings forms a reduced clearance with the housing, which restricts the flow of the processed mixture. This restriction leads to a rapid increase in the pressure and friction within the mixture, resulting in a temperature rise. Forcing the feed mixture through the compression gates also promotes homogenization. Within their zone, the gates accelerate the processes occurring in the mixture and reduce the cycle time of the material passage. This acceleration allows for shortening the length of each screw section, as the necessary processing completes over a shorter distance without compromising the extrusion quality [25]. To test the hypothesis that the process improvement and acceleration in each screw section depend on the geometric shape and axial length of the compression rings, the axial length of the rings is varied, and the cylindrical shape is replaced with a conical one. This modification reduces the volume of the compression ring and increases the volume available for the mixture, which is a positive factor since this volume cannot be recirculated through the screw casing, but instead contributes directly to forward movement [26].

The pressure P_p required to force the extruded mixture through a conical compression gate ring is to be determined. The feed material is advanced by the screw from left to right under the action of force Px, and is compressed into the reduced clearance due to the conical shape of the compression rings, as depicted in Figure 7. For an elementary layer of the extruded mixture with thickness dx, a differential equilibrium equation is formulated along the X-axis:

$$P_x\pi(r_0^2 - r_x^2) - (P_x + dP)\pi(r_0^2 - r_x^2) - F_{tr0} - F_{trx}\cos\alpha - P_{bx}2\pi r_x dl\sin\alpha = 0 \quad (10)$$

where Px is the pressure at the current elementary section of the compression ring (Pa), F_{tr0} and F_{trx} are the friction forces on the wall of the cylinder and the compression ring,

respectively (N), P_{bx} is the lateral pressure on the wall of the compression ring (Pa), *rx* is the radius of the current section of the compression ring (m), r_0 is the inner radius of the cylindrical housing of the extruder screw (m), and α is the convergence angle of the conical longitudinal surface of the compression ring (degrees).

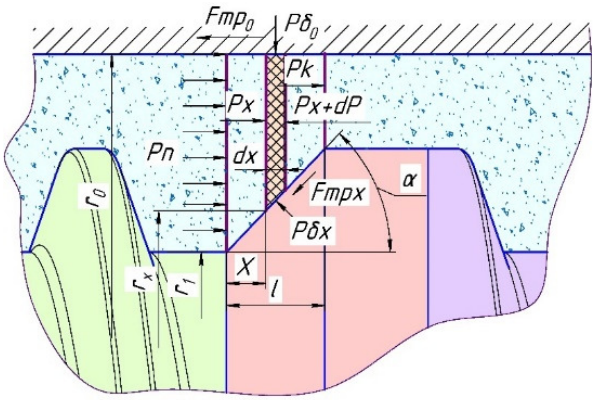

Fig. 7. Material flow through the compression gate ring in the screw assembly of the extruder.

The friction force is calculated using the corresponding lateral pressure:

$$F_{tr0} = 2\pi r_0 dx f P_{b0} \quad (11)$$

$$F_{trx} = 2\pi r_x \cdot dl \cdot f \cdot P_{bx} \quad (12)$$

where P_{b0} is the lateral pressure on the wall of the cylindrical housing of the extruder screw (Pa).

Using the layer thickness *dx* and the cone angle α of the compression ring, the elementary width of the selected conical surface section is expressed as:

$$dl = \frac{dx}{cos\alpha} \quad (13)$$

For the same surface with thickness *dx*, a differential equilibrium equation is formulated along the vertical Y-axis:

$$P_{b0} 2\pi r_0 dx - P_{bx} 2\pi r_x dl cos\alpha + F_{trx} = 0 \quad (14)$$

After transformations based on (14) and (12), the following variables are obtained:

$$P_{b0} = \frac{P_{bx} r_x (1 - ftg\alpha)}{r_0} \quad (15)$$

$$P_{bx} = \xi \times P_x \quad (16)$$

$$F_{tr0} = 2\pi r_x \xi \cdot P_x dx f (1 - ftg\alpha) \quad (17)$$

The differential equilibrium equation for the selected portion of the mixture with thickness *dx*, along the horizontal X-axis, is written as:

$$dP\pi(r_0^2 - r_x^2) - 2\pi r_x \xi P_x dx f (1 - ftg\alpha) - 2\pi r_x dx f \xi P_x - P_{bx} 2\pi r_x dx tg\alpha = 0 \quad (18)$$

At a distance *x* from the edge of the compression ring, the radius is determined according to Figure 5 as:

$$r_x = r_1 + x \cdot tg\alpha \quad (19)$$

where r_1 is the initial radius of the conical compression ring (m), and *X* is the distance from the beginning of the ring to the elementary section *dx* (m).

Substituting (19) into (18) and integrating the result, yields the pressure value at any point along the conical compression ring:

$$P_x = \frac{P_k}{\left(\frac{(r_1 + ltg\alpha)^2}{r_1^2 - r_0^2}\right)^{0,5\xi\left(\frac{2f}{tg\alpha} - 1 - f^2\right)}} \quad (20)$$

Using (20), the compaction pressure at the entrance to the conical compression ring is determined, where l_k is the length of the compression ring (m):

$$P_{p\kappa} = \frac{P_k}{\left(\frac{(r_1 + l_k tg\alpha)^2}{r_1^2 - r_0^2}\right)^{0,5\xi\left(\frac{2f}{tg\alpha} - 1 - f^2\right)}} \quad (21)$$

Using (21), a graphical dependence of the required compaction pressure in front of the conical compression gate ring on its axial length is constructed, as depicted in Figure 8. (for ξ = 0.43, f = 0.4, P_k = 1.05 MPa, r_1 = 0.014 m, and r_0 = 0.019 m).

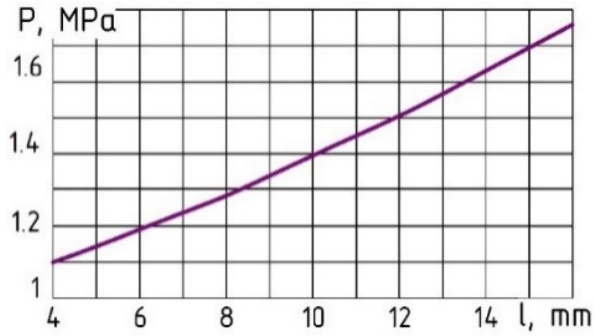

Fig. 8. Variation of compaction pressure in front of the compression gate ring as a function of its length l_k.

As shown in Figure 8, an increase in the axial length l_k of the conical compression gate ring leads to a rise in pressure in front of the ring, which, in turn, results in an increase in the overall average pressure and temperature. For each extruded feed mixture, a compression ring with the most optimal parameters can be preselected. The obtained theoretical dependencies allow the determination of the required pressure acting on the extruded material at any desired point within the housing of the screw assembly. The extrusion pressure in front of the die is determined using (8), and the pressure in front of the compression rings is calculated using (21). The pressure generated by the screw flight crests is assumed to increase linearly along the length of the screw, which makes it possible to derive the relationships for calculating the pressure retained after the compression gate rings, denoted as P_{k1} and P_{k2}:

$$P_{k1} = \frac{P_{p2} \cdot l_1}{l_1 + l_2} \quad (22)$$

$$P_{k2} = \frac{P_p(l_1+l_2)}{l_1+l_2+l_3} \quad (23)$$

where l_1, l_2, and l_3 are the lengths of the first, second, and third screw sections.

The pressure at any point along the screw can be calculated as:

$$P_{x,n} = \frac{(P_{pn}-P_{kn})\cdot l}{l_n} \quad (24)$$

where P_{pn} is pressure in front of the compression ring at the end of the n^{th} screw section (Pa), P_{kn} is the pressure at the beginning of the compression ring in the n^{th} screw section (Pa), l is the distance from the beginning of the screw to the designated pressure calculation point (m), and l_n is the total length of the n^{th} screw section.

Figure 9 schematically presents the pressure development stages along the entire length of the screw within the housing of the screw assembly.

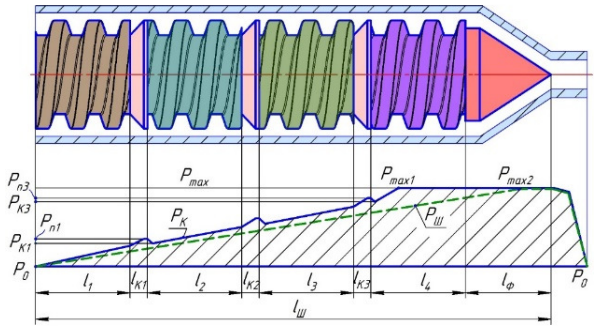

Fig. 9. Pressure variation in the extruder with and without conical compression rings.

Preliminary theoretical studies of the relationship between the extrusion pressure within the screw housing and the structural features of the screw assembly confirmed the significant influence of the length of the forming head, the cross-sectional area S_{otv} of the die opening, and the axial length of the compression rings on the overall average pressure. Equations (8), and (21-23) make it possible to determine the pressure at any point along the screw assembly of the extruder. The use of conical compression rings accelerates the increase in the average pressure and potentially the temperature of the processed mixture over a shorter screw length. This is undoubtedly an advantage over cylindrical rings and allows shortening the final section of the screw–and therefore the entire screw–if necessary.

According to the existing hypothesis, an increase in the mixture temperature may also be promoted by enlarged friction surfaces on the extruder screw. This is due to the increased frictional work, e.g., of the feed mixture mass between the screw flights and the rising pressure at the locations of the compression rings, which collectively contribute to a rise in temperature [27, 28]. The friction surface area on the screw can be increased by designing the screw flights in a double-start configuration, i.e., two helical threads rotating around the shaft, as exhibited in Figure 10.

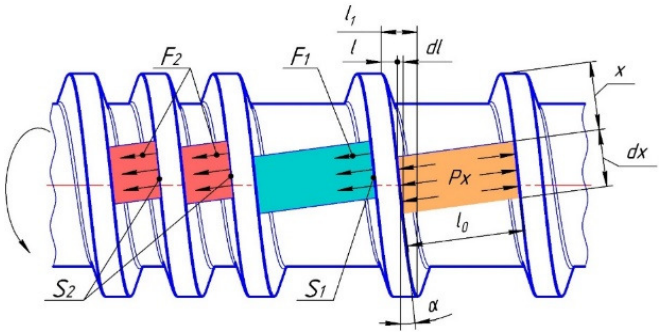

Fig. 10. Visual comparison of parameters between double-start and single-start screws: F1 – forces acting on the material in a single-start screw, F2 – forces acting on the material in a double-start screw, S1 - contact area between the material and the flight of a single-start screw, S2 - contact area between the material and the flight of a double-start screw.

The work of the friction force in the first segment of the inter-flight channel can be expressed using a known relationship [17]:

$$A_1 = \int_0^{l_1} F_{tr}dx \quad (25)$$

$$A_1 = \int_0^{l_1} \frac{(P_{n1}-P_0)l}{l_1} \times \frac{l\mu(2h_V+l_V)}{sin\alpha\cdot tg\alpha} dl \quad (26)$$

By integrating this expression, the equation for the friction work in the first section of the screw is obtained:

$$A_1 = \frac{l_1^2\mu(2h_{v1}+l_{v1})(2P_{n1}+P_0)}{6sin\alpha_1\cdot tg\alpha_1} \quad (27)$$

The total friction work of a three-section composite screw shaft is determined by summing the friction work in each individual screw section:

$$\sum A = A_1 + A_2 + A_3 \quad (28)$$

$$\sum A = \frac{l_1^2\mu(2h_{v1}+l_{v1})(2P_{n1}+P_0)}{6sin\alpha_1\cdot tg\alpha_1} + \frac{l_2^2\mu(2h_{v2}+l_{v2})(2P_{n2}+P_{k1})}{3sin\alpha_2\cdot tg\alpha_2} + \frac{l_3^2\mu(2h_{v3}+l_{v3})(2P_{n3}+P_{k2})}{3sin\alpha_3\cdot tg\alpha_3} \quad (29)$$

After performing the transformations, the following formulas are obtained for calculating the mass of the mixture in each of the three sections of the extruder:

$$M_1 = \rho\frac{l_1}{T_1}\left(t_1\cdot\pi\cdot(2h_{v1}r_{vH1} - h_{v1}^2) - 2\delta_{v1}h_{v1}t_1\sqrt{1+ctg\alpha_1}\right) \quad (30)$$

$$M_2 = \rho\frac{l_2}{T_2}\left(t_2\cdot\pi\cdot(2h_{v2}r_{vH2} - h_{v2}^2) - 2\delta_{v2}h_{v2}t_2\sqrt{1+ctg\alpha_2}\right) \quad (31)$$

$$M_3 = \rho\frac{l_3}{T_3}\left(t_3\cdot\pi\cdot(2h_{v3}r_{vH3} - h_{v3}^2) - 2\delta_{v3}h_{v3}t_3\sqrt{1+ctg\alpha_3}\right) \quad (32)$$

where t_1, t_2, and t_3 are the pitch in the corresponding section of the extruder screw (m), r_{vn1}, r_{vn2}, and r_{vn3} are the outer radius of the flight in the respective section of the extruder screw (m), and δ_{v1}, δ_{v2}, δ_{v3} are the flight width in the corresponding screw section (m).

By performing the necessary transformations, the total mass of the mixture contained within the screw flights is obtained:

$$\sum M = \rho(\frac{l_1}{t_1}\left(t_1 \cdot \pi \cdot (2h_{v1}r_{vH1} - h_{v1}^2) - 2\delta_{v1}h_{v1}t_1\sqrt{1 + ctg\alpha_1}\right) + \frac{l_2}{t_2}\left(t_2 \cdot \pi \cdot (2h_{v2}r_{vH2} - h_{v2}^2) - 2\delta_{v2}h_{v2}t_2\sqrt{1 + ctg\alpha_2}\right) + \frac{l_3}{t_3}\left(t_3 \cdot \pi \cdot (2h_{v3}r_{vH3} - h_{v3}^2) - 2\delta_{v3}h_{v3}t_3\sqrt{1 + ctg\alpha_3}\right)) \quad (33)$$

The temperature of the mixture during processing is significantly influenced by the pressure within the screw assembly of the extruder. This pressure can be predicted in advance by selecting compression rings of different lengths and shapes or by subsequently adjusting the cross-sectional area of the die outlet.

The influence of the changes in the axial length and shape of the compression rings is illustrated graphically in Figure 11(a), while the influence of the cross-sectional area of the die opening on the overall temperature of the feed mixture inside the screw assembly is depicted in Figure 11(b), based on the following parameters of the PE-150 extruder: screw pitch $t_1 = t_2 = t_3 = 20$ mm, screw lengths $l_1 = 160$ mm, $l_2 = l_3 = 135$ mm, outer radius of screw flights $r_{vn1} = r_{vn2} = r_{vn3} = 37$ mm, axial lengths of compression rings $l_{1k} = 4$ mm, $l_{2k} = 8$ mm, $l_{3k} = 12$ mm, $l_{4k} = 16$ mm, and extrusion pressure before the die $P_p = 0{,}92$ MPa.

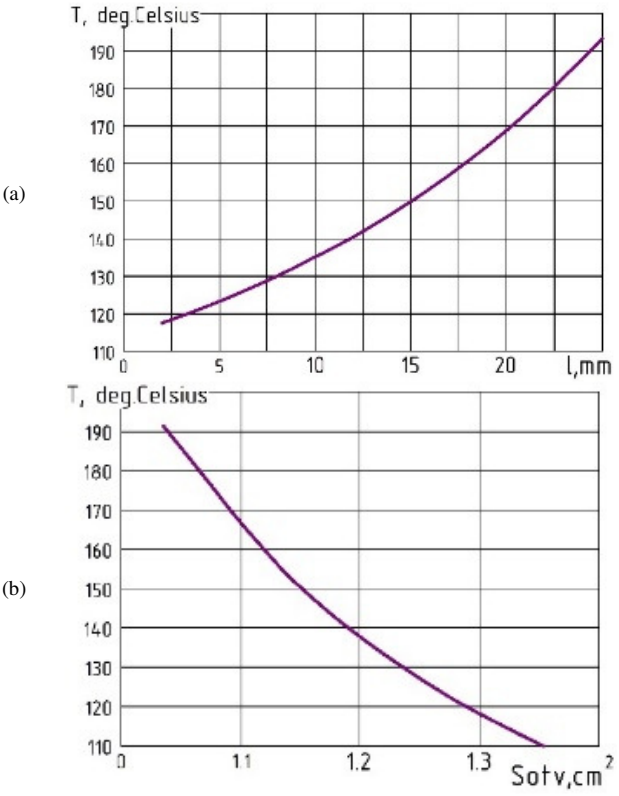

Fig. 11. Influence of the axial length l of the compression ring: (a) on the cross-sectional area S_{otv} of the die opening, (b) on the temperature change of the mixture inside the screw assembly.

The analysis of the data points in Figure 11(a) demonstrates that the length of the compression rings significantly affects the pressure within the screw assembly. Figure 11(b) exhibits that the larger the cross-sectional area S_{otv} of the die opening is, the lower is the temperature in the screw zone. Thus, during operation, by tightening the die, thereby changing the cross-sectional area, it becomes possible to adjust not only the pressure, but also the desired temperature within the screw zone.

Next, the extruder throughput was calculated, since it serves as an important confirmation of the machine's performance efficiency. As the feed mixture enters the screw zone, it is ground, compressed through the compression ring seals, melted, and propelled toward the die outlet. With equal screw pitch in all sections, the lowest efficiency and throughput occurs at the initial transport zone, which ultimately determines the throughput of the entire extruder. The throughput is calculated by multiplying the mass of the mixture in a single flight of the first screw section by the time per revolution [17]:

$$Q_t = m \cdot \frac{\omega}{2\pi} \quad (34)$$

$$m = \rho \times v \quad (35)$$

where m is mass of the processed mixture in a single screw flight (kg), and Q_t is the theoretical throughput of the extruder screw (kg/s).

The theoretical throughput of the grain extruder is determined as:

$$Q_T = \rho \cdot \left(t\pi(2h_v r_{vH}) - 2\sigma_v h_v t\sqrt{1 + ctg^2\alpha}\right)\frac{\omega}{2\pi} \quad (36)$$

When calculating the throughput of the grain extruder, it is important to consider that not all materials reach the die in a single pass. The extrusion process is characterized by a forced backflow of the mixture that fails to pass through the compression rings and is returned via the grooves in the housing, then recaptured by the screw. The operational throughput of the prototype extruder is given by:

$$Q_e = Q_T \cdot \left(1 - \frac{P_{p1}}{P_{max}}\right) \quad (37)$$

$$P_{max} = \frac{\pi r_{vH}^2 \omega \eta z}{2(r_{vH} - r_k)T} \quad (38)$$

where P_{max} is the maximum pressure generated by the screw in the absence of axial movement of the mixture, with the extruder die closed, and η is the effective viscosity of the mixture.

By substituting (38) and (36) into (37) and performing the necessary transformations, the desired operational throughput of the prototype extruder is obtained:

$$Q_e = \rho\left(t\pi(2h_v r_{vH}) - 2\sigma_v h_v t\sqrt{1 + ctg^2\alpha}\right)\frac{\omega}{2\pi} \cdot \left(1 - \frac{P_{p1}2(r_{vH} - r_k)t}{\pi r_{vH}^2 \omega \eta z}\right) \quad (39)$$

Using (38) and the data provided in Figure 11, a graph was plotted to illustrate the increase in the throughput with an increase in the cross-sectional area S_{otv} of the die opening, as depicted in Figure 12(a), as well as its additional adjustment

through the changes in the screw rotation frequency, screw pitch, and screw radius, as presented in Figure 12(b).

(a)

(b)

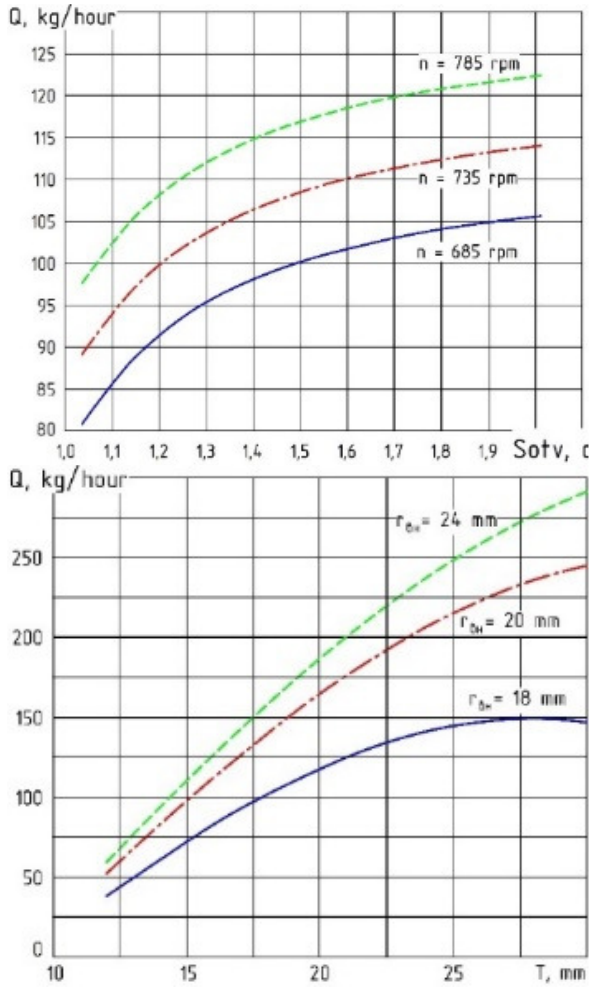

Fig. 12. Change in extruder throughput based on: (a) an increase in the cross-sectional area S_{ov}, (b) screw rotation frequency, screw pitch, and screw radius.

The graph in Figure 12(a) logically demonstrates the increase in the throughput as the screw rotation frequency and die outlet area increase. However, this process is not without limitations: the excessive opening of the die results in the interruption of the extrusion process, as the pressure and temperature of the mixture fall below the required levels.

Figure 12(b) illustrates the dependence of the extruder throughput on the structural screw parameters—namely, the pitch and radius of the screw flights. As the screw pitch increases, the throughput increases up to a certain point, after which it begins to decline, most likely due to the increased resistance in the compression rings and the enhanced recirculation of the feed mixture within the extruder. An increase in the screw radius also leads to a rise in the throughput.

To compare the performance of the prototype extruder with other machines in the same category, the specific energy consumption formula was applied, and Figure 13 was constructed to show the effect of the temperature in the screw assembly on specific energy consumption.

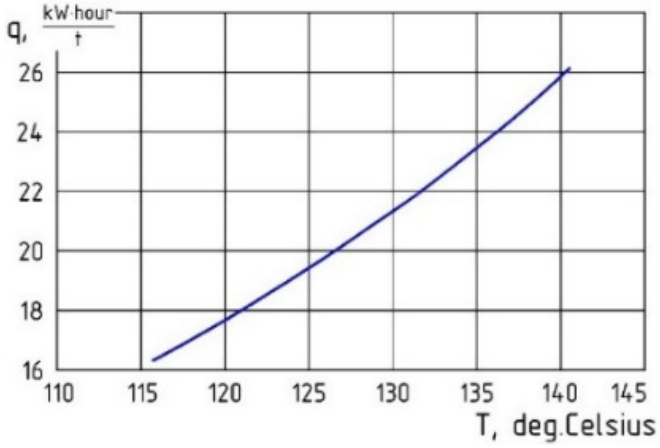

Fig. 13. Relationship between specific energy consumption and the temperature of the feed mixture thermal processing in the extruder's screw assembly.

As portrayed in Figure 13, an increase in the temperature within the screw assembly leads to higher specific energy consumption. Therefore, a rational solution would be the installation of compression rings of various designs on the screw shaft, enabling the required temperature increase to be achieved over a shorter screw length, while maintaining the energy consumption.

As mentioned earlier, modifying the screw pitch in the transport zone can also enhance the extruder throughput, but excessive pitch may cause the blockage of the screw with the mixture in the narrowed gap area above the conical compression ring and the housing. To prevent such blockage, it is necessary to accurately determine the pitch increase limit.

III. RESULTS.

To validate the mathematical relationships and obtain real operational data of the extruder, experimental studies were conducted. To reduce costs, a special laboratory setup was developed at LLP SPA Innotech based on the full-scale grain extruder PE-150.

The extruded material consisted of a plant-coniferous mixture containing 87% grain filler, 10% crushed crop waste (sunflower stalks and heads), and 3% crushed Siberian fir needles.

The working part (screw unit) of the extruder, shown in Figure 14, includes the screw shaft 1 uniting all screw sections, housing 2, die head 3, housing of the n-th screw section 4, feeding screw section 5, compression rings 6, die plate 7, conical shaft head 8, fastening clamps 9, and hopper 10.

The process of grain extrusion proceeds as follows (Figure 14): the feed mixture is dosed from hopper 10 onto the feeding section of the screw 5, gradually compressed and transported to the first compression ring 6; the operation is then repeated in

the next section. During transportation, due to friction and compression, the mixture is flattened, pressed, and heated. The compression rings 6 create increased resistance to movement, elevated pressure, and a rise in temperature. The gap between the conical shaft head 8 and the die head 3 with die plate 7 also regulates the pressure, temperature, and the discharge rate of the material through the die opening 7.

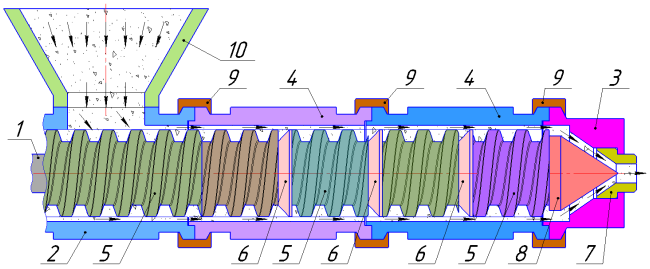

Fig. 14. Process of grain extrusion.

According to the conclusions of the theoretical analysis, the productivity of the grain extruder is significantly influenced by the screw rotation speed, pitch, and the radius of the screw flights, as seen in Figures 10 and 11. The pitch of the transport section of the screw can be increased by up to 1.4 times without causing blockage. For the experiment, screw sections of different lengths were manufactured, allowing for an easy replacement in case of failure—either replacing a short screw section with another short one, or one long section with two short ones. Figure 15 shows the designs of the screw sections.

Fig. 15. Designs of screw sections of various lengths for the extruder.

The experimental verification of the influence of the design and the parameters of the screw unit on the performance indicators of the extruder operation was conducted in accordance with a multifactor experimental plan. A rotatable, three-level second-order Box–Behnken design for three factors was selected, originally developed to analyze the relationship between the input and output parameters. The operational screw rotation frequency range, 685–785 rpm, was chosen for an expected product output of 95–110 kg/h. The cross-sectional area, as shown in Figures 12 and 13 was set at S_{otv} = 1.2 cm². The screw pitch was t = 20 mm, and the external screw flight radius was r_{vn1} = 18 mm.

According to Figure 11, the die outlet area S_{otv} = 1.2 cm² corresponds to a temperature of 120–140 °C, achieved through the use of compression rings with a length of (4–12) mm. Screw sections for the experiment were manufactured with pitches of 18, 24, and 28 mm. The tests were carried out under steady-state operating conditions in accordance with the developed plan. The chosen output parameters were: temperature, productivity, and power consumption. The values of T (°C), Q (kg/h), and N (kW) are given as the average values obtained from three repeated tests. As a result of the multifactor regression analysis conducted based on the experimental data, a relationship was established between the temperature of the extruded mixture (T °C) and the corresponding factors: screw rotation speed n, rpm (X_1); length of the compression rings h, mm (X_2); and the pitch of the transport screw section t, mm (X_3). Several experimental series were carried out; the insignificant factor values were excluded. Based on the stable data, a regression equation was developed, representing a full quadratic model that adequately approximates the experimental results with a significance level of $\alpha = 0.05$:

$$T = -197{,}10 + 0{,}8427 \cdot X_1 + 0{,}6563 \cdot X_2 - 0{,}0535 \cdot X_3 - 0{,}00057 \cdot X_1^2 + 0{,}08125 \cdot X_2^2 - 0{,}00552 \cdot X_3^2 \quad (40)$$

The response surface showing the relationship of the temperature (T °C) in the screw zone on the compression ring length h and screw rotation speed n (rpm), based on the regression model, is presented in Figure 16.

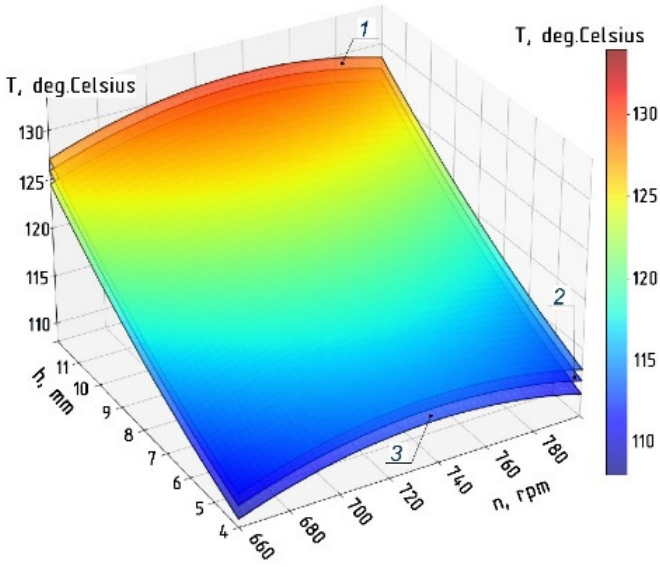

Fig. 16. Variation of temperature T (°C) with screw rotation speed n (rpm) and compression ring length h (mm) at a fixed screw pitch t (mm) in the transport section.

In Figure 16, three planes are superimposed: the top plane (1) corresponds to a pitch t = 20 mm; the middle plane (2) corresponds to t = 24 mm; and the bottom plane (3) corresponds to t = 28 mm. The response surface showing the relationship of the temperature (T °C) in the screw zone on the pitch (t) of the transport screw section and the length (h) of the compression ring, based on the regression model, is displayed in Figure 17. Similarly, three planes are superimposed: the top plane (1) corresponds to a rotation speed n = 785 rpm; the middle plane (2) corresponds to n = 735 rpm; and the bottom plane (3) corresponds to n = 685 rpm.

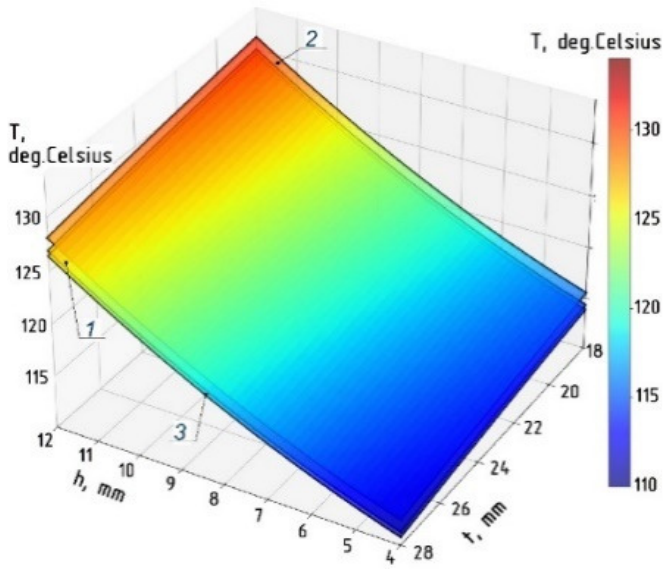

Fig. 17. Variation of temperature T (°C) with compression ring length h (mm) and screw pitch t (mm) in the transport section at a fixed screw rotation speed n (rpm).

The most efficient thermal regime (120–140 °C) in the screw zone, according to the constructed response surface, is achieved when compression rings with a longitudinal length of 7–12 mm are installed and the screw pitch in the transport section is set to 20 mm. When this pitch increases to 28 mm, the required thermal regime is attained with compression rings 9–12 mm in length. Moreover, as the longitudinal length of the compression ring increases, the temperature in the corresponding screw zone also rises. An increased screw pitch leads to a slight temperature decrease. Under the examined conditions, the rotation speed has almost no effect on the temperature in the screw zone.

The next relationship, obtained after regression analysis of the data from a repeated experiment, adequately approximates its results at a significance level of $\alpha = 0.05$. It excludes the insignificant effects and describes the change in the output capacity Q (kg/h) depending on the following factors: screw rotation speed n (rpm) (X_1), compression ring length h (mm) (X_2), and screw pitch t (mm) of the transport section (X_3).

$$Q = -171.47 - 0{,}2228 \cdot X_1 + 14{,}5225 \cdot X_2 + 17.4487 \cdot X_3 + 0{,}000015 \cdot X_1^2 + 0{,}0015 \cdot X_1 \cdot X_2 + 0{,}01888 \cdot X_1 \cdot X_3 - 0{,}193 \cdot X_2^2 - 0{,}7344 \cdot X_2 \cdot X_3 - 0{,}4539 \cdot X_3^2 \quad (41)$$

A graphical representation of the response surface illustrating the change in the extruder output capacity (Q) as a function of the corresponding factors—screw rotation speed (n) and screw pitch (t) of the transport section—based on the results of the regression analysis, is illustrated in Figure 18. Three response surfaces are superimposed: the top surface (1) corresponds to a pitch t = 28 mm, the middle surface (2) corresponds to t = 24 mm, and the bottom surface (3) corresponds to t = 20 mm.

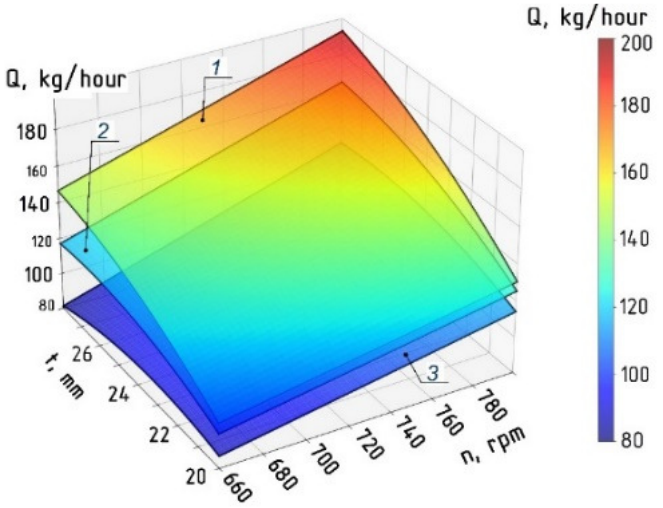

Fig. 18. Variation of output capacity Q (kg/h) with extruder shaft rotation speed n (rpm) and compression ring length h (mm) at a fixed screw pitch t (mm) in the transport zone.

A graphical representation of the response surface illustrating the change in the extruder output capacity (Q) as a function of the relevant factors – compression ring length (h) and screw pitch (t) based on the regression analysis results, is shown in Figure 19. The three superimposed response planes are arranged as follows: the top surface (1) corresponds to a rotation speed n = 785 rpm, the middle surface (2) to n = 735 rpm, and the bottom surface (3) to n = 685 rpm.

The analysis of the response surface confirms that the maximum output capacity primarily depends on the changes in the screw pitch and rotation speed. Increasing the axial length of the compression ring affects the output less significantly than it does the temperature and pressure, as it induces backflow and reverse movement of the mixture through the return channels in the housing. Increasing the screw pitch or its rotation speed leads to higher extruder productivity.

The constructive and technological parameters ensuring the maximum output capacity of Q = 135 kg/h—while maintaining the recommended process temperature—were determined as follows: compression ring length h = 8 mm, and screw pitch in the transport section t = 24 mm. The average experimental productivity range was 100–135 kg/h.

A multifactor regression analysis conducted on the experimental results also revealed the dependence of the power consumed (N, kW) in the extrusion of the feed mixture on the selected factors: screw rotation speed (n, rpm) (X_1),

compression ring length (h, mm) (X_2), and screw pitch in the transport section (t, mm) (X_3). The regression analysis led to an equation that adequately approximates the experimental results at a significance level of $\alpha = 0.05$:

$$N = 2{,}735654 - 0{,}004685 \cdot X_1 + 0{,}012739 \cdot X_2 - 0{,}004756 \cdot X_3 + 0{,}000005 \cdot X_1^2 + 0{,}000062 \cdot X_1 \cdot X_2 - 0{,}000018 \cdot X_1 \cdot X_3 + {,}001875 \cdot X_2^2 - 0{,}001287 \cdot X_2 \cdot X_3 + 0{,}000365 \cdot X_3^2 \quad (42)$$

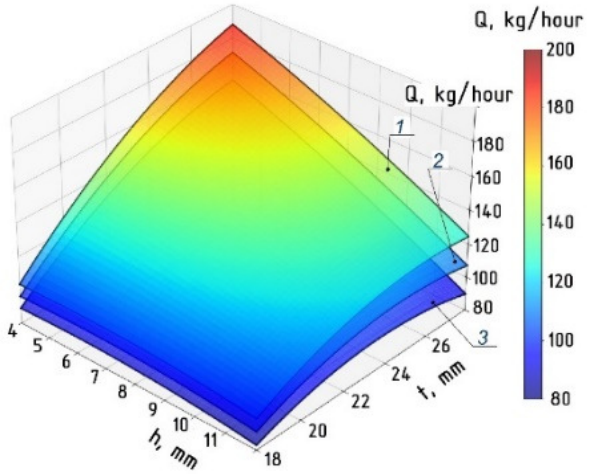

Fig. 19. Variation of output capacity Q (kg/h) with compression ring length h (mm) and screw pitch t (mm) in the transport zone at a fixed extruder shaft rotation speed n (rpm).

The response surface characterizing the changes in the consumed power (N) during the experiment, as influenced by the axial length (h) of the compression ring and the screw rotation speed (n), based on the results of the regression analysis, is shown in Figure 20.

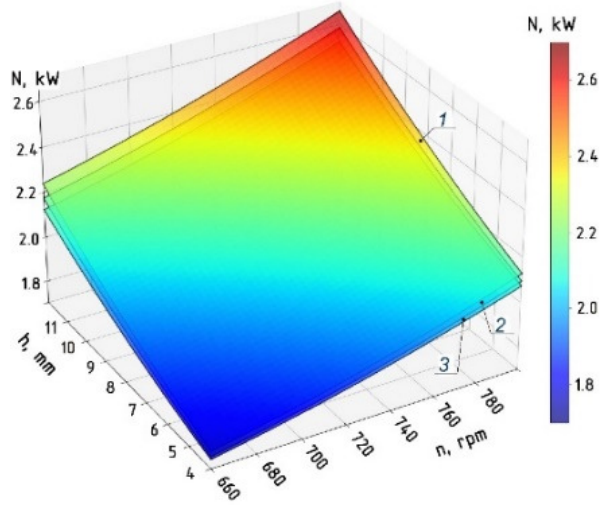

Fig. 20. Power consumption N (kW) as a function of extruder shaft rotation speed n (rpm) and compression ring length h (mm) at a fixed screw pitch t (mm) in the transport zone.

The three response surfaces overlaid in the Figure 20 almost merge, yet exhibit slight distinctions and are arranged in the following order: the upper surface (1) corresponds to a screw pitch of t = 20 mm, the middle surface (2) to t = 24 mm, and the lower surface (3) to t = 28 mm. The analysis of the response surfaces confirms the theoretical dependencies of the power consumption on all selected factors: screw rotation speed (n), screw pitch (t), and axial length (h) of the compression ring. An increase in the axial length (h) of the compression ring leads to an increase in the power consumption (N). In contrast, an increase in the screw pitch (t) reduces the power consumption. A rise in the screw rotation speed (n) increases the power consumption. During the experiment, the power consumption ranged from 1.94 kW to 2.53 kW.

IV. CONCLUSION

The theoretically substantiated and experimentally validated constructive and technological parameters of the screw assembly of a grain extruder enable an accurate and predictable selection of the optimal design parameters during the modernization of the grain extrusion equipment. The use of compression rings of varying lengths allows achieving the required processing temperature and extrusion pressure over a shorter screw length. The most effective extruder configuration involves the use of a double-start screw with an increased pitch in the feeding zone and conical compression rings.

Optimal processing conditions ensuring the highest feed quality are achieved with the following parameters: compression rings with an initial radius of r_1 = 14 mm, final radius r_2 = 16 mm, and length l = 8 mm; double-start screw with a crest radius r_{vn1} = 18 mm, tooth height 4 mm, screw pitch t = 20 mm, transport zone length 60 mm, compaction zone 35 mm, pressing zone 35 mm, and screw rotation speed n = 785 rpm. The most effective method for adjusting the processing temperature is by changing the cross-sectional area of the die opening.

ACKNOWLEDGMENT

This research was funded by the Science Committee of the Ministry of Science and Higher Education of the Republic of Kazakhstan (grant AR23485224 – Development of new energy-efficient equipment for the production of innovative feed additives for livestock using industrial waste).

DATA AVAILABILITY

The dataset and related experimental data are available from the corresponding author upon reasonable request.

REFERENCES

[1] K. E. Mironov *et al.*, " Development and Study of the Grain Crushing Working Process of Shocking and Reflective Crusher," *Vestnik of Kazan State Agrarian University*, vol. 14, no. 1, pp. 100–106, Mar. 2019, https://doi.org/10.12737/article_5cceddbcce1e93.58919071.

[2] X. Mu, H. Li, Z. Wang, Q. Wang, D. Geng, and J. Zhu, "Comparison of Crushing Effect of Differently Shaped Crushing Rollers on Whole-Plant Silage Maize," *Agriculture*, vol. 13, no. 7, June 2023, Art. no. 1276, https://doi.org/10.3390/agriculture13071276.

[3] Penza State Technological University *et al.*, "Justification of a Promising Functional Scheme of a Grain Crusher," *Bulletin Samara State*

Agricultural Academy, vol. 9, no. 2, pp. 34–43, May 2024, https://doi.org/10.55170/1997-3225-2024-9-2-34-43.

[4] S. Y. Bulatov, "Modeling of Work Process of Grain Crusher Ejector," *Traktory i sel hozmashiny*, vol. 82, no. 5, pp. 25–27, May 2015, https://doi.org/10.17816/0321-4443-65437.

[5] O. F. Kraugerud and B. Svihus, "Effects of Online Pretreatment of Plant Ingredients on Processing Responses and Physical Properties in Extruded Fish Feed," *Animal Feed Science and Technology*, vol. 168, no. 3–4, pp. 250–256, Sept. 2011, https://doi.org/10.1016/j.anifeedsci.2011.04.089.

[6] V. Kushnir, N. Gavrilov, and T. Shkotova, "Improvement of the Extruder Construction," in *Proceedings of the 4th International Conference on Industrial Engineering*, A. A. Radionov, O. A. Kravchenko, V. I. Guzeev, and Y. V. Rozhdestvenskiy, Eds., Springer International Publishing, 2019, pp. 2133–2142.

[7] H. Li, Z. Xiong, and X. Li, "Optimization of the Extrusion Process for the Development of Extruded Snacks Using Peanut, Buckwheat, and Rice Blend," *Journal of Food Processing and Preservation*, vol. 43, no. 12, Dec. 2019, https://doi.org/10.1111/jfpp.14264.

[8] A. Kabdusheva, A. Kurmanov, M. Amantayev, Y. Khasenov, and V. Sapa, "The Effect of Parameters on the Performance Efficacy of a Single Screw Feed Extruder Using a Design Experiments and Response Surface Methodology," *Bulgarian Journal of Agricultural Science*, vol. 26, no. 2, pp. 492–497, 2020.

[9] Q. Liu, Y. X. He, W. W. Sun, T. T. Ji, and S. Zhuang, "Effect of Enzyme Supplementation and Extruding Process on the Digestibility of Nutrients and Phenolic Acids of Defatted Rice Bran Based Diets in Ileal-cannulated Growing Pigs," *Livestock Science*, vol. 240, Oct. 2020, Art. no. 104138, https://doi.org/10.1016/j.livsci.2020.104138.

[10] J. Amft, J. L. Bauer, J. Rostek, S. Spielvogel, and K. Schwarz, "Effect of Water Addition on the Microstructure, Lipid Incorporation, and Lipid Oxidation of Corn Extrudates," *European Journal of Lipid Science and Technology*, vol. 121, no. 9, Sept. 2019, Art. no. 1800433, https://doi.org/10.1002/ejlt.201800433.

[11] V. Y. Frolov, E. A. Kotelevskaya, and M. I. Tumanova, "Theoretical Aspects of the Working Process of a Press Extruder with a Variable Step Auger for Preparation of Concentrated Feed," *IOP Conference Series: Earth and Environmental Science*, vol. 548, no. 5, Aug. 2020, Art. no. 052003, https://doi.org/10.1088/1755-1315/548/5/052003.

[12] A. Likunov, "New Technology of the Steel Fiber Manufacturing from Technogenic Waste," *International Journal of Mechanical and Production Engineering Research and Development*, vol. 10, no. 3, pp. 611–622, 2020.

[13] L. A. Adache, T. S. Mogaji, M. O. Olayinka, and Z. A. Olagoke, "Design and Finite Element Analysis of an Extractor Machine for Castor Oil Biodiesel Production," *Journal of Applied Research in Technology & Engineering*, vol. 6, no. 1, pp. 34–50, Jan. 2025, https://doi.org/10.4995/jarte.2025.21917.

[14] S. Yadav, A. K. Jha, and H. B. Darlami, "Design and Improvement of Dewatering System Implemented for Biogas Slurry," *International Journal for Multidisciplinary Research*, vol. 5, no. 6, Dec. 2023, Art. no. 9184, https://doi.org/10.36948/ijfmr.2023.v05i06.9184.

[15] S. A. Karrab and M. A. Ballem, "Failure Analysis and Repair of a Broken Extruder Shaft," *European Journal of Engineering Research and Science*, vol. 5, no. 1, pp. 107–111, Jan. 2020, https://doi.org/10.24018/ejers.2020.5.1.1738.

[16] O. Lyashuk *et al.*, "Fracture Cause Analysis of the Extruder's Shaft and Geometry Optimization of the Spline," *Journal of Mechanical Engineering and Sciences*, vol. 13, no. 1, pp. 4449–4460, Mar. 2019, https://doi.org/10.15282/jmes.13.1.2019.08.0378.

[17] M. Doudkin, A. Kim, M. Młyńczak, G. Kustarev, and V. Kim, "Development and Parameter Justification of Vibroscreen Feed Elements," in *Mining Machines and Earth-Moving Equipment*, M. Sokolski, Ed. Springer International Publishing, 2020, pp. 203–226.

[18] S. L. Li and J. Lu, "Finite Element Analysis of Worm Auger in Meat Grinder," *Advanced Materials Research*, vol. 945–949, pp. 162–165, June 2014, https://doi.org/10.4028/www.scientific.net/AMR.945-949.162.

[19] P. Pareek and K. Madloi, " Ansys Analysis on Screw Conveyor Employing Diverse Coating Materials," *International Journal of Emerging Technologies and Innovative Research*, vol. 9, no. 6, pp. d36–d48, June 2022.

[20] O. Lyashuk, M. Sokil, V. Klendiy, O. Skyba, and V. Dmytrenko, "Study on Nonlinear Model of Dynamics of a System 'Extruder Elastic Auger Working Body,'" *Acta Technologica Agriculturae*, vol. 19, no. 4, pp. 101–106, Dec. 2016, https://doi.org/10.1515/ata-2016-0020.

[21] B. Hu, F. Cao, and Z. Xing, "Numerical Study on Rotor Deformation of Multiphase Twin-screw Pumps Under High Gas Volume Fraction Conditions," in *the International Compressor Engineering Conference*, Purdue, West Lafayette, IN, USA, Jul. 2012, Art. no. 2143.

[22] W. E. Abdel-Ghany, S. J. Ebeid, and I. Fikry, "Mechanical Design Aspects of Single Screw Extruders Using Finite Element Analysis," *International Journal of Engineering and Technical Research*, vol. 3, no. 7, pp. 47–52, July 2015.

[23] V. I. Pakhomov *et al.*, "Results of experimental studies of the process of joint extrusion of forage grain and green mass of alfalfa," *Processes and Machines of Agro-Engineering Systems*, no. 9, pp. 45–48, 2017, https://doi.org/10.24412/1997-0749-2017-9-45-48.

[24] Z. Y. Tian *et al.*, "Optimization and Characteristic Analysis of Screw Rotor of a Twin-screw Pump," *Journal of Vibroengineering*, vol. 25, no. 1, pp. 171–188, Feb. 2023, https://doi.org/10.21595/jve.2022.22545.

[25] A. M. Bizhanov, "Mathematical Modeling of Extrusion Agglomeration," *Metallurgist*, vol. 67, no. 9–10, pp. 1362–1372, Jan. 2024, https://doi.org/10.1007/s11015-024-01628-2.

[26] K. Kombayev, A. Kim, D. Yelemanov, and G. Sypainova, "Strengthening of Low-Carbon Alloy Steel by Electrolytic-Plasma Hardening," *International Review of Mechanical Engineering*, vol. 16, no. 2, Feb. 2022, Art. no. 84, https://doi.org/10.15866/ireme.v16i2.21712.

[27] A. Kim, G. Guryanov, A. Vavilov, A. Bugayev, and Y. Doudkina, "Development of Mounted Impact-Rotor Working Equipment for Destruction of Snow-Ice Formations," *International Review of Mechanical Engineering*, vol. 15, no. 5, May 2021, Art. no. 258, https://doi.org/10.15866/ireme.v15i5.20805.

[28] A. T. Nguyen *et al.*, "Determination of Best Input Parameters for Internal Grinding SKD11 Tool Steel using MCDM," *Engineering, Technology & Applied Science Research*, vol. 15, no. 1, pp. 20190–20196, Feb. 2025, https://doi.org/10.48084/etasr.9505.